

Senior Thesis

A Novel Approach to Phosphoproteomic Mutant-Wildtype Comparative Analysis as Applied to the T-Cell Activation Pathway

Norris Hung
Science Bachelors in Biology
Brown University

Submitted to the Department of Biology
for the partial fulfillment of Honors

April 2009

TABLE OF CONTENTS

0 Acknowledgements	p3
1 Introduction	p4
2 Methods	p9
3 Results	p15
4 Discussion	p19
5 References	p25
6 Figure Legends	p33
7 Figures	p38
8 Appendix I	p46

Acknowledgements

If it seems that the quality and quantity of effort amounted to in this paper is more than can be performed by one undergraduate over the course of a little more than a year, the assumption is correct. The methodology of the approach had largely been perfected by the work of graduate student, Vinh Nguyen, and former undergraduate, Johnathan T. Lin, before I had begun my research. When I joined the lab near the end of Spring 2008, the major tasks of validating the approach and its utility still remained. In this thesis, I strive to focus on my individual contribution although some discussion of previous work is inevitable.

My role in this could not have succeeded if it were not for the patient mentoring and enormous assistance of Vinh Nguyen – not simply on this project, but on life in general. For this, I am truly indebted. In the same light, I am deeply grateful to Professor Arthur Salomon for his guidance, continual belief in my work, and for always pushing me to work harder. In addition, I would like to thank Kebin Yu for his constant help with the technological side of things, Lulu Cao for her consultation and advice with experiments, and Anna Ritz for her site-clustering algorithm. Indeed, the entire team of the Salomon Lab has provided a fun and engaging environment that I only hope my future destinations can match.

Lastly, I would like to thank my parents for their unfathomable sacrifice and support – for without them, I could not have gotten to where I am today.

Chapter 1 Introduction

The Field of Phosphoproteomics

Proteomics is an emerging field of system-wide biology that seeks to study various aspects of proteins on a large-scale. The core technology of proteomics is the mass spectrometer, which allows for rapid and sensitive ability to generate spectra from protein fragments. When coupled with protein and genomic databases, this technology provides a powerful tool for high-throughput analysis of proteins.

Many research applications of proteomics include protein interaction, post-translational modifications, and protein profiling. In particular, phosphoproteomics has been an important development. While protein phosphorylation is the best understood post-translational modification, traditional 2-D gel-based methods of phosphoprotein isolation and analysis, such as phosphate-labeling and western blot detection, are not able to provide definitive evidence of phosphorylation. (1) However, because mass spectrometry is able to accurately detect mass of peptide fragments, not only can it confidently identify phosphoproteins, but it can assign the phosphorylated amino acid residue. (1)

As phosphorylation plays an important role in kinase/phosphatase signaling cascades, phosphoproteomics can offer detailed insights into the function and placement of proteins in cellular pathways. Due to the ephemeral nature of phosphorylation events, time course quantitation experiments provide a critical means of studying phosphorylation patterns. By triggering a pathway then analyzing the protein lysates

from specific time points after activation, we are able to, in a sense, take snapshots of how the entire cell responds to the activation of that pathway. For example, for proteins that function earlier in a simple pathway, we would expect higher levels of phosphorylation in earlier time points and less phosphorylation at later time points. By the same logic, proteins downstream would be expected to have higher phosphorylation levels at later time points.

A Novel Approach

While time course experiments can help to provide hints to placement of proteins in a pathway, its resolution is still low and dependent on the amount of time points considered. Even if a snapshot of the system can be achieved every 30 seconds, the number of proteins in a complex signaling pathway that function in each time window will still likely to be dense. In addition, because pathways are not in isolation in the cell, phosphorylation noise from other activities in the cell may often cause difficulties in determining whether increased phosphorylation actually correlates with a pathway or whether it is simply background.

Combining time course experiments with more controlled genetic knockout studies would allow for more precise placement of proteins within a pathway. By knocking out a specific protein of interest, we can look for changes that occur in phosphorylation of any other given protein in the phosphoproteome. However, if only one time point is considered, the results can completely miss the timeframe of an phosphorylation event of a particular protein. Combining both quantitative techniques

can provide a powerful tool not only for protein placement but also discovery of novel protein functions and interactions.

This three-dimension study of phosphorylation across protein, time, and phenotype presents a technical challenge of quantification across all three variables. In order to relate levels of phosphorylation between each time point experiment, a quantification method is necessary to compare relative amounts of proteins between samples. A separate quantification method must also be used to compare phosphorylation levels across mutant and wild-type phenotypes. The utility of such an approach depends significantly on carefully choosing the appropriate quantitation techniques. Currently, there are four common methods of quantitation: metabolic labeling (SILAC), chemical labeling (ICAT), absolute quantitation (AQUA), and label-free techniques. (2)

Metabolic labeling, introduces stable isotope-labeled amino acids into the cell during growth and division; this is known as stable-isotope labeling by amino acids in cell-culture (SILAC). Because labeling and sample combination can occur early on in an experiment, SILAC is the most accurate labeling-based quantitation. However, due to the limit of available isotopes, the major drawback of SILAC is that the comparison of a maximum of three experiments can be made. (2). This quantitation method, while would not be ideal for time course comparisons, can provide an accurate means to quantifying phosphoproteins between mutant and wild-type phenotypes.

In order to provide the highest resolution of proteins, a large number of time points will be necessary. However, because quantitation techniques involving isotope labeling are limited to the amount of isotopes available, comparisons are generally

limited to 2-3 states. (2) Label-free techniques involving normalization to spiked phosphopeptide standards, however, can theoretically provide comparisons between an infinite number of states. By combining SILAC and label-free quantitation techniques, we can accurately compare proteome-wide phosphorylation levels between wild-type and mutant cells across a dense array of time points.

T-Cell Activation as a Model

In order to assess the utility of this phosphoproteomic approach, the activation pathway in helper T-cells was chosen as a test bed because of detailed level of prior characterization. Helper T-cells play an essential role in the immune system by recognizing foreign antigen presented by a variety of antigen presenting cells (APCs) and releasing extracellular cytokines such as IL-2. The availability of the Jurkat leukemic T cell line has greatly facilitated investigations of TCR signaling by traditional and phosphoproteomic methods (3, 4). Furthermore, many isogenic disruption mutants of essential TCR signaling proteins that reveal severe phenotypic defects in TCR signaling and function have been isolated through genetic screens of Jurkat clones (5-9). In particular, P116, a well-characterized Zap-70 null clone, displays defects in stimulus-induced calcium mobilization, IL-2 production, NFAT transcription activation, and protein tyrosine phosphorylation on PLC- γ 1, Itk, LAT, Erk1/2, and SLP76 (8, 10-12).

In the present study, a hybrid SILAC/label free approach was applied to the P116 (Zap-70 null) and P116.c139 (Zap-70 reconstituted to wild type levels) Jurkat clones, and the placement of newly discovered tyrosine phosphorylation sites relative to Zap-70 was determined. (Figure 1) In addition to the validation of this approach by overlaying

results on the canonical t-cell activation pathway, the collected data has allowed for the generation of novel hypotheses of protein interaction involving proteins such as Fyn, SKAP55, and NTBA. These hypotheses, while cannot be verified by this approach alone, can serve as starting points for future genetic or biochemical experiments.

Chapter 2 Methods

Cell Culture and SILAC Labeling

Jurkat P116 (Zap-70 null) and Jurkat P116.c139 (Zap-70 reconstituted) cell lines were grown in RPMI 1640 at 37°C in 250 ml culture flasks supplemented with 10% heat-inactivated dialyzed fetal bovine serum, 100 µg/ml penicillin and 100 µg/ml streptomycin. After 5 days in regular RPMI media, cells were washed twice with RPMI lacking Arg and Lys. Zap-70 reconstituted cells were reconstituted in RPMI with $^{12}\text{C}_6$ / $^{14}\text{N}_4$ Arg and $^{12}\text{C}_6$ / $^{14}\text{N}_2$ Lys (light media). Zap-70 null cells were reconstituted in $^{13}\text{C}_6$ / $^{15}\text{N}_4$ Arg and $^{13}\text{C}_6$ / $^{15}\text{N}_2$ Lys (heavy media).

Stimulation and Lysis

After 2 passages in SILAC labeled media, cells were washed in 4°C PBS and reconstituted at a concentration of 1×10^8 cells/ml in 4°C PBS. Cells were divided into 1ml aliquots each to correspond to one replicate of one time point. Each aliquot was then combined with 2.5 µg/ml OKT3 and 2.5 µg/ml OKT4 antibodies and placed at 4°C for 10 minutes. Cell aliquots were then crosslinked with 12.2 µg/ml goat anti-mouse IgG and transferred to 37°C for either 0, 1, 2, 3, 5, 7, or 10 minutes. To stop further propagation of the cascade, cells were lysed in lysis buffer (8M Urea, 1 mM sodium orthovanadate, and 100mM pH 8.0 Ammonium Bicarbonate) and placed at 4°C for 20 minutes.

Replicates

Replicate experiments were done either as technical replicates or biological replicates. In total, 5 replicates were performed: one biological replicate containing 2 technical replicates and another biological replicate containing 3 technical replicates. Technical replicates were combined after cell lysis.

SILAC Light and Heavy Combination

A lowry assay was performed to determine protein concentration of all lysate samples. Zap-70 reconstituted lysates(light) and Zap-70 null lysates(heavy) of each time point were then combined at a 1:1 ratio.

Protein Processing

Reduction → Alkylation → Trypsin Digestion → Desalt

Lysates were reduced with 10mM DTT at 56°C for 1 hour and alkylated with 1mM iodoacetamide at room temperature for 1 hour in the dark. Lysates were then diluted five-fold with pH 8.9 100mM ammonium bicarbonate and digested with trypsin overnight at 1:100 trypsin to protein ratio. After digestion, samples were acidified to pH 2 by HCl titration and desalted using c18 Sep-Pak plus cartridges and lyophilized in a Speed-Vac.

Addition of Synthetic Standardization Peptide

100 pmol of synthetic phosphopeptide LIEDAEpYTAK was added to each sample.

Phosphotyrosine Enrichment

Dry peptides from each time point were reconstituted and immunoprecipitated as previously described (13) except 20 μ l of anti-phosphotyrosine resin was used per 1×10^8 cells and eluted peptides were filtered through a 0.22 μ M filter.

Automated Desalt/IMAC and Mass Analysis

Tryptic peptides were analyzed by a fully automated phosphoproteomic technology platform integrating peptide desalting via reversed-phase chromatography, and Fe³⁺ IMAC enrichment of phosphopeptides as previously described (13). IMAC enriched phosphopeptides were eluted into the mass spectrometer (LTQ-FT; Thermo Fisher Scientific) through an analytical column (360 μ m OD X 75 μ m ID fused silica with 12 cm of 5 μ m Monitor C18 particles with an integrated ~4 μ m ESI emitter tip fritted with 3 μ m silica; Bangs Laboratories) with a reversed-phase gradient (0-70% solvent B in 30 min). Static peak parking was performed via flow rate reduction from 200 nl/min to ~20 nl/min when peptides began to elute as judged from a BSA peptide scouting run, as described previously (14). Using a split flow configuration, an electrospray voltage of 2.0 kV was applied, as described (15). Spectra were collected in positive ion mode and in cycles of one full MS scan in the FT (m/z: 400-1800), followed by data-dependent MS/MS scans in the LTQ (~0.3 s each) sequentially of the five most abundant ions in each MS scan with charge state screening for +1, +2, +3 ions and dynamic exclusion time of 30 s. The automatic gain control was 1,000,000 for the FTMS scan and 10,000 for the ion trap MS (ITMS) scans. The maximum ion time was 100 ms for the ITMS scan and 500 ms for the FTMS full scan. FTMS resolution was set at 100,000.

MS/MS spectra were searched against the human National Center for Biotechnology Information non-redundant protein database using the SEQUEST algorithm provided with Bioworks 3.2 (SEQUEST v.27 rev12) (16). Peak lists were generated using Bioworks 3.2 (extract_msn.exe 11/27/06) using a mass range of 600-4500, precursor ion tolerance (for grouping) of 0.005 AMU, minimum ion count of 5, group scan of 0, minimum group count of 1. The NCBI human database contained 489,388 protein entries (50% forward, 50% reversed). SEQUEST was performed with the following parameters: trypsin enzyme specificity, 2 possible missed cleavages, 0.2 Da mass tolerance for precursor ions, 0.5 Da mass tolerance for fragment ions. Search parameters specified a differential modification of phosphorylation (+79.9663 Da) on serine, threonine, and tyrosine residues and a static modification of carbamidomethylation (+57.0215 Da) on cysteine. Search parameters also included a differential modification for arginine (+10.00827 Da) and lysine (+8.01420 Da) amino acids. To provide high confidence phosphopeptide sequence assignments, SEQUEST results were filtered by Xcorr (+1 > 1.5; +2 > 2.0; +3 > 2.5), precursor mass error (<20 ppm), and a logistic spectral score (17) that assessed MS/MS spectral quality (> 0.7981), minimum peak area threshold of 500 SILAC and label free quantitation were required, non-redundant phosphopeptides, and proteins with descriptors of "unnamed" or "unknown" were removed. Additionally, repeat observations of MS/MS spectra of each tyrosine phosphorylated peptide in minimally three of six total time points were required. False discovery rate was estimated with the decoy database approach after

final assembly of nonredundant data into heatmaps (18). To validate the position of the phosphorylation site, the Ascore algorithm (19) was applied to all data and the reported phosphorylation site position reflects the top Ascore prediction.

Quantitation of relative phosphopeptide abundance

Relative quantitation of peptide abundance was performed via calculation of selected ion chromatogram (SIC) peak areas of heavy and light SILAC labeled peptides. For label free comparison of phosphopeptide abundance in the Zap-70 reconstituted Jurkat cells, individual time point SICs were normalized to the LIEDAEPYTAK peak area in the same timepoint. The standard exogenous LIEDAEPYTAK peptide accompanied cellular phosphopeptides through the peptide immunoprecipitation, desalt, IMAC, and reversed-phase elution into the mass spectrometer. Peak areas were calculated by inspection of SICs using recently developed software programmed in Microsoft Visual Basic 6.0 based on Xcalibur Development Kit 2.0 SR2 (Thermo Fisher Scientific). Quantitative data was calculated automatically for every assigned peptide using the ICIS algorithm available in the Xcalibur XDK with the following parameters: multiplet resolution of 8, noise tolerance of 0.1, noise window of 40, scans in baseline of 5, include of RefExc peaks False. A minimum SIC peak area equivalent to the typical spectral noise level of 500 was required of all data reported for label free and SILAC quantitation.

Western Blotting

Total cell lysates were diluted 1:1 with gel loading buffer (4% SDS, 125 mM pH6.8 Tris-HCl, 20% glycerol, 5% 2-mercaptoethanol, .01% bromophenol blue). Equal protein

concentrations measured by Lowry Assay were separated by SDS-page and electroblotted to an Imobilon membrane. The membrane was blocked for 45 minutes in PBS/Tween-20 with 5% milk at 22°C and then incubated at 4°C for 12 hours 1:1000 of either rabbit anti-human phospho-p44/p42 MAPK (Thr202/Tyr204) or mouse anti-human Zap-70 antibody. Membrane was then washed 4x10 minutes at 22 °C in PBS/Tween-20. Membrane was then stained with 1:3000 of anti-rabbit IgG or anti-mouse IgG directly conjugated to horseradish peroxidase for 1 hour in blocking buffer at 22 °C and washed 5x15 minutes with PBS/Tween-20. Bands were visualized using chemiluminescence with the ECL+ kit.

Chapter 3 Results

Zap-70 null T-cells and Zap-70 reconstituted T-cells were respectively labeled with SILAC light and heavy amino acids. The cells were stimulated for 0, 2, 3, 5, 7, or 10 minutes and then lysed to stop stimulation. Stable isotope labeled Zap-70 null and Zap-70 reconstituted lysates of each time point were then combined and processed. The label-free normalization peptide was added in equal concentrations to each time point and phosphotyrosine peptides were enriched for by both anti-phospho-Tyr IP and IMAC. (Figure 2)

From mass analysis, 169 unique tyrosine phosphotyrosine sites dispersed throughout 134 proteins were detected from this experiment. Out of these 169 sites, 31 have previously been associated with the T-cell signaling pathway including CD3 subunits $\gamma\delta\epsilon\zeta$; tyrosine kinases Lck, Fyn, and Zap-70; crucial adaptor proteins LAT, Itk, PLC γ 1; and downstream target proteins PI3K, Erk1, Erk2, CD5.

Based on the known canonical T-cell signaling pathway, we expect that phosphorylation sites of proteins will show different patterns depending on their existence or placement in the pathway. Generally, we expect that sites on proteins downstream of Zap-70 to show lower phosphorylation levels due to Zap-70 removal. Sites that show no change in phosphorylation levels may either function upstream of Zap-70 or may not function in the pathway at all. Elevated phosphorylation may be due to misregulation of a protein; for instance, a protein can show increased level of phosphorylation due to decreased activity of an inhibitor.

In order to assess the validity of this approach, phosphorylation sites were clustered into 3 different categories based on the change of phosphorylation levels between Zap-70 null and Zap-70 reconstituted cells. (Figure 3)

Decreased Phosphorylation in Response to Zap-70 Removal

34 phosphorylation sites showed a slight decrease in phosphorylation defined as 2-10x reduction on 4 or more time points. 16 sites showed significantly decreased phosphorylation defined as greater than 10x reduction on 4 or more time points. As expected, many key downstream proteins such as PLC- γ 1 (Y⁷⁷¹ and Y⁷⁷⁵), ERK1 (Y²⁰⁴), ERK2 (Y¹⁸⁷), and LAT (Y⁴⁵) reside in this cluster. Previous studies have also shown decreased tyrosine phosphorylation on these proteins. (20, 21, 22)

Many immunoreceptor tyrosine activation motif (ITAM) phosphorylation sites of the T-cell receptor also exhibited decreased phosphorylation including CD3 δ (Y¹⁶⁰ and Y¹⁴⁹), CD3 ζ (Y¹¹¹ and Y¹⁴²), and CD3 ϵ (Y¹⁹⁹ and Y⁷²). While this was unexpected because these proteins are upstream of Zap-70, a literature search nonetheless reveals that these results are consistent with previous studies. While Lck mediated phosphorylation of CD3 ζ ITAMs is widely believed to precede Zap-70 recruitment and activation (23), previous studies have revealed a synergistic role of Zap-70 mediated recruitment as well as stabilization of the interaction between Lck and CD3 ζ at the ITAM regions independent of Zap-70 kinase activity. (Figure 5A) (24, 25) Additional reports have indicated an essential role of Lck in the regulation of constitutive phosphorylation of CD3 ζ (26). From these studies, it can be proposed that the removal of Zap-70 would

result in a decrease of CD3 ζ basal phosphorylation levels, which is consistent with our findings on these sites.

Elevated Phosphorylation in Response to Zap-70 Removal

Of the 169 total detected sites, 59 showed elevated phosphorylation in Zap-70 null cells, which was defined as greater than 2x induction on two or more time points. In general, elevation of phosphorylation in response to Zap-70 removal could be caused by decreased activity of a phosphatase downstream of Zap-70. Many phosphatases are believed to have a prominent role in T-cell activation, which may explain the high number of sites with elevated phosphorylation; however, their functions are largely speculative and the placement of many of these phosphatases are unknown. (27) While our results do not show any conclusive data on misregulation events, they can allow us to generate hypothesis of potential tyrosine phosphatases. One such hypothesis to explain the drastic increase in phosphorylation of Fyn (Y⁴²⁰) is included in the discussion section. Furthermore, there are likely other possible rationales for elevated phosphorylation such as disruption of protein turnover mechanisms that should be explored.

No Change in Phosphorylation in Response to Zap-70 Removal

Of the 169 total detected sites, 26 sites show no change in phosphorylation defined as 0-2 fold change in 4 or more time points. This cluster included proteins known to function upstream of Zap-70 (CD3 ϵ , CD3 ζ , Lck) (28), proteins known to

function in other signaling pathways in T cells (GSK3 β , PAG) (29, 30), and ones not known to function in TCR signaling (Filamin B, CDC2, ELMO1).

Novel Phosphorylation Sites

Among the 179 total unique phosphorylation sites identified in this analysis, 96 of these sites were previously not known to have been phosphorylated. (Figure 6) Furthermore, of the 96 novel sites, phosphorylation levels of 57 of these sites were significantly altered with Zap-70 removal indicating a possible role in the T-cell activation pathway. Further research is needed to confirm and determine the role of these novel sites.

Chapter 4 Discussion

Current quantitative phosphoproteomic approaches have been recruited to either make comparisons between different states of a system or to make temporal comparisons. Time course experiments can provide a timelapse view of phosphorylation events in a single system but cannot provide detailed information about placement of proteins in a pathway. Comparisons between mutant and wild-type cells can provide a high resolution picture of where a protein functions but can be easily misguided if analyzed phosphoproteins were obtained outside of their phosphorylated time frame. A logical marriage of the two quantitative techniques provides a multi-dimensional and synergistic view of the phosphoproteome and can be imperative in elucidation of pathways.

The complementarity of our results to existing knowledge on the T-cell signaling pathway provides strong evidence of the validity of our approach. As expected, many of the key downstream proteins showed a decrease in phosphorylation in Zap-70 null cells compared to Zap-70 reconstituted cells. In addition, many of the proteins that fell into the “no change” category were either not known to perform in the T-cell signaling pathway or functioned upstream of Zap-70. Some of the results were initially unexpected, such as the increased phosphorylation of sites in the ITAM region, but these data merely spoke of the inherent complexity of the T-cell signaling pathway. While quantitative phosphoproteomics can provide a means to overcome many limitations of typical pathway elucidation approach, this fact serves as a reminder that the analysis phosphoproteomics can be complicated by complex pathway interactions and is an issue

that still needs to be addressed. In addition, the existence of positive/negative feedback pathways and mutant compensation mechanisms should also be considered when interpreting phosphoproteomic data.

Hypothesis Generation

Interesting data, such as newly discovered phosphorylation sites or surprising phosphorylation events in response to protein removal, allows for the generation of hypothesis concerning protein placement or function. In particular, our results have generated some unexpected hypotheses about the potential role of tyrosine phosphatases in the differential regulation of the Src type kinases Lck and Fyn (Figure 7). Misregulation of protein tyrosine phosphatase α (PTP α) could explain the elevated phosphorylation seen in response to Zap-70 removal on Fyn Y420 and known Fyn targets such as Y169 and Y90 on SIT (31) yet relative small change in phosphorylation on Lck Y505. Previous studies revealed that Fyn activity is elevated in the absence of PTP α in primary thymocytes (32), and that the activity of PTP α is regulated by 3 phosphorylation sites (S180, S204, and Y798) (33, 34). PTP α activation occurs through formation of a complex with PI3K and PKC δ , with subsequent phosphorylation of S180 and S204 by PKC δ independently of Y798 phosphorylation (33, 34, 35) Furthermore, PTP α selectively regulates Fyn over other Src family kinases such as Lck, dephosphorylating Fyn at both Y420 in the activation loop and the c-terminal inhibitory site Y53. (32, 36) Our data is consistent with the hypothesis that the removal of Zap-70 leads to a decrease in phosphorylation on the activation site Y313 of PKC δ as well as Y228 of PI3K, causing a reduction in PTP α activity (through the lack of phosphorylation on S180 and S204),

leading to an increase in Fyn Y420 phosphorylation and phosphorylation of the Fyn substrate SIT at Y169 and Y90. Although we observed the phosphorylation on site Y798 of PTP α to be unaffected in response to Zap-70 removal, defects in phosphorylation on S180 and S204 of PTP α may be the cause of selective Fyn misregulation.

We also observed a novel site found in the Pleckstrin homology domain (PH domain) of SKAP55 (Y142). This site was observed to have slightly enhanced phosphorylation (significantly increased at 3 and 10 minutes, p-value < 0.05) in Zap-70 null cells compared to its reconstituted counterpart in response to stimulation. Upon T cell activation, Fyn-associated SKAP55, in complex with the cytosolic adaptor protein ADAP, targets RAP1 GTPase to the plasma membrane to initiate cell adhesion (37-39). While the mechanisms of SKAP55's interaction with Fyn and ADAP are well studied, the specific regulatory mechanisms of SKAP55's membrane targeting is still uncharacterized (37, 38). It has been established that the PH domain is involved in membrane recruitment for many cellular proteins (40). More recently, it has been shown that tyrosine phosphorylation of the PH domain of protein kinase D can serve in regulating protein function by possibly releasing the PH domain (undefined still whether it is from itself or the membrane), leading to its activation (41). Therefore, we hypothesize that phosphorylation at Y142 of SKAP55 may lead to the inhibition of SKAP55's ability bind to the membrane, which would prevent RAP1 GTPase recruitment to the membrane and cell adhesion. The placement of a negatively charged phosphate group in the PH domain could impede the ability of SKAP55 to bind to polyphosphoinositides found at

the membrane (40). The enhanced phosphorylation of Y142 on SKAP55 could be explained by the misregulation of Fyn, a known regulator of SKAP55 (37, 39).

Our results also provide some insight on the possible function of NTBA in T cells. NTBA, an ITIM containing killer Ig-like receptor (KIR), has been previously shown to be expressed in all human NK, T and B lymphocytes (42, 43). In NK cells, NTBA has been shown to display inhibitory functions by blocking the ability of NK cells to kill Epstein-Barr Virus-infected target cells (42). Little is known about their role in T cells. Recently, certain KIRs (KIR2DL2 and KLRG1) have been shown to disrupt late T cell receptor stimulated effector functions such the production of IFN- γ and IL-2, respectively (44, 45). Furthermore, site-directed mutagenesis of specific tyrosine residues in the ITIM motif of KLRG1 demonstrates the importance of tyrosine phosphorylation in the inhibitory process in T cells (45). In our results, the phosphorylation of site Y308 located within the ITIM motif of NTBA was increased (significantly increased at 7min, p-value < 0.05) in response to TCR crosslinking in Zap-70 reconstituted Jurkat cells, suggesting the involvement of NTBA in the T cell activation pathway. It is possible that NTBA, like other KIRs, functions to inhibit late T-cell signaling events through phosphorylation of Y308. Additionally, we observed a slightly decreased phosphorylation (significantly decreased at 7 minutes, p-value < 0.05) of Y308 in Zap-70 null cells suggesting that this site may be downstream of Zap-70 activation.

Some complications arose during the course of this study, some unavoidable and some that may serve as an important note for future experiments. Specifically, our label-

free data was not able to separate protein phosphorylation events temporally to a high resolution. While some of the cause may be due to current sensitivity limits of the mass spectrometer, a likely problem is that our density and spacing of time points were not able to capture the range of phosphorylation in the pathway. Subsequent T-cell receptor stimulation assays by graduate student (Lulu Cao) in our lab has shown that inclusion of time points between 1 and 3 minutes at a 30 second interval can provide adequate temporal separation of phosphorylation events. Another complication encountered is that fact that not all proteins of the t-cell activation pathway were discovered. However, this is an inherent obstacle in current mass spectrometry technology; only the top 5 proteins at be sampled during one scan and the ability to detect a protein is determined by the quality of prior separation and the ability of a protein to hold a charge. We expect at as this technology continues to improve, more phosphoproteins will be captured within one experiment

The quantitative phosphoproteomic isogenic mutant approach described here will not only provide greater insights into molecular mechanisms of the TCR signaling pathway, but also provide a generalized approach to elucidation of cell signaling pathways using phosphoproteomics. Although current phosphoproteomic studies have been impressive in their identification and quantitation of changes in phosphorylation abundance across large numbers of proteins (46-50), the development of methodology capable of the multi-dimensional comparison of mutant and wild type cells through a time course of receptor stimulation is critically important. By combining genetic analysis and two well-established proteomic quantitation methods, our approach facilitates rapid

elucidation of the biological significance of high throughput phosphoproteomic data. Comparison of data from removal of multiple signaling proteins at different positions within a single pathway (upstream, middle, and downstream) will provide a means of organizing hundreds to thousands of phosphorylation sites relative to canonical pathway signaling landmarks. Although our hybrid quantitation approach was applied to the analysis of wide-scale tyrosine phosphorylation here, it is generic in design and adaptable to a wide range of phosphopeptide enrichment strategies. Quantitative phosphoproteomic phenotyping of signaling protein mutants will be an ideal complement to traditional signaling approaches, accelerating understanding of the architecture of phosphorylation networks involved in a wide range of biological processes.

Chapter 5 References

- (1) Reinders, J. and A. Sickmann, State-of-the-art in phosphoproteomics. *Proteomics*, 2005. 5(16): p. 4052-61.
- (2) Bantscheff, M., et al., Quantitative mass spectrometry in proteomics: a critical review. *Anal Bioanal Chem*, 2007. 389(4): p. 1017-31.
- (3) Salomon, A. R., Ficarro, S. B., Brill, L. M., Brinker, A., Phung, Q. T., Ericson, C., Sauer, K., Brock, A., Horn, D. M., Schultz, P. G., and Peters, E. C. (2003) Profiling of tyrosine phosphorylation pathways in human cells using mass spectrometry. *Proc Natl Acad Sci U S A* 100, Page 443-8.
- (4) Abraham, R. T., and Weiss, A. (2004) Jurkat T cells and development of the T-cell receptor signalling paradigm. *Nat Rev Immunol* 4, Page 301-8.
- (5) Finco, T. S., Kadlecsek, T., Zhang, W., Samelson, L. E., and Weiss, A. (1998) LAT is required for TCR-mediated activation of PLCgamma1 and the Ras pathway. *Immunity* 9, Page 617-26.
- (6) Irvin, B. J., Williams, B. L., Nilson, A. E., Maynor, H. O., and Abraham, R. T. (2000) Pleiotropic contributions of phospholipase C-gamma1 (PLC-gamma1) to T-cell antigen receptor-mediated signaling: reconstitution studies of a PLC-gamma1-deficient Jurkat T-cell line. *Mol Cell Biol* 20, Page 9149-61.
- (7) Straus, D. B., and Weiss, A. (1992) Genetic evidence for the involvement of the lck tyrosine kinase in signal transduction through the T cell antigen receptor. *Cell* 70, Page 585-93.

- (8) Williams, B. L., Schreiber, K. L., Zhang, W., Wange, R. L., Samelson, L. E., Leibson, P. J., and Abraham, R. T. (1998) Genetic evidence for differential coupling of Syk family kinases to the T-cell receptor: reconstitution studies in a ZAP-70-deficient Jurkat T-cell line. *Mol Cell Biol* 18, Page 1388-99.
- (9) Yablonski, D., Kuhne, M. R., Kadlecsek, T., and Weiss, A. (1998) Uncoupling of nonreceptor tyrosine kinases from PLC-gamma1 in an SLP-76-deficient T cell. *Science* 281, Page 413-6.
- (10) Shan, X., and Wange, R. L. (1999) Itk/Emt/Tsk activation in response to CD3 cross-linking in Jurkat T cells requires ZAP-70 and Lat and is independent of membrane recruitment. *J Biol Chem* 274, Page 29323-30.
- (11) Martelli, M. P., Lin, H., Zhang, W., Samelson, L. E., and Bierer, B. E. (2000) Signaling via LAT (linker for T-cell activation) and Syk/ZAP70 is required for ERK activation and NFAT transcriptional activation following CD2 stimulation. *Blood* 96, Page 2181-90.
- (12) Griffith, C. E., Zhang, W., and Wange, R. L. (1998) ZAP-70-dependent and -independent activation of Erk in Jurkat T cells. Differences in signaling induced by H₂O₂ and Cd3 cross-linking. *J Biol Chem* 273, Page 10771-6.
- (13) Cao, L., Yu, K., Banh, C., Nguyen, V., Ritz, A., Raphael, B. J., Kawakami, Y., Kawakami, T., and Salomon, A. R. (2007) Quantitative time-resolved phosphoproteomic analysis of mast cell signaling. *J Immunol* 179, Page 5864-76.
- (14) Ficarro, S. B., Salomon, A. R., Brill, L. M., Mason, D. E., Stettler-Gill, M., Brock, A., and Peters, E. C. (2005) Automated immobilized metal affinity chromatography/nano-

liquid chromatography/electrospray ionization mass spectrometry platform for profiling protein phosphorylation sites. *Rapid Commun Mass Spectrom* 19, Page 57-71.

(15) Licklider, L. J., Thoreen, C. C., Peng, J., and Gygi, S. P. (2002) Automation of nanoscale microcapillary liquid chromatography-tandem mass spectrometry with a vented column. *Anal Chem* 74, Page 3076-83.

(16) Eng, J., A. McCormack, J. R. Yates. (1994) An approach to correlate tandem mass spectral data of peptides with amino acid sequences in a protein database. . *J. Am . Soc. Mass Spec.* 5, Page 976-989.

(17) Yu, K., Sabelli, A., DeKeukelaere, L., Park, R., Sindi, S., Gatsonis C.A., and Salomon, A.R. (2009) Integrated platform for high-throughput statistical and manual validation of tandem mass spectra. *Proteomics* In Press.

(18) Elias, J. E., and Gygi, S. P. (2007) Target-decoy search strategy for increased confidence in large-scale protein identifications by mass spectrometry. *Nat Methods* 4, Page 207-14.

(19) Beausoleil, S. A., Villen, J., Gerber, S. A., Rush, J., and Gygi, S. P. (2006) A probability-based approach for high-throughput protein phosphorylation analysis and site localization. *Nat Biotechnol* 24, Page 1285-92.

(20) Williams, B. L., Schreiber, K. L., Zhang, W., Wange, R. L., Samelson, L. E., Leibson, P. J., and Abraham, R. T. (1998) Genetic evidence for differential coupling of Syk family kinases to the T-cell receptor: reconstitution studies in a ZAP-70-deficient Jurkat T-cell line. *Mol Cell Biol* 18, Page 1388-99.

- (21) Shan, X., and Wange, R. L. (1999) Itk/Emt/Tsk activation in response to CD3 cross-linking in Jurkat T cells requires ZAP-70 and Lat and is independent of membrane recruitment. *J Biol Chem* 274, Page 29323-30.
- (22) Martelli, M. P., Lin, H., Zhang, W., Samelson, L. E., and Bierer, B. E. (2000) Signaling via LAT (linker for T-cell activation) and Syk/ZAP70 is required for ERK activation and NFAT transcriptional activation following CD2 stimulation. *Blood* 96, Page 2181-90.
- (23) Wange, R. L., and Samelson, L. E. (1996) Complex complexes: signaling at the TCR. *Immunity* 5, Page 197-205.
- (24) Steinberg, M., Adjali, O., Swainson, L., Merida, P., Di Bartolo, V., Pelletier, L., Taylor, N., and Noraz, N. (2004) T-cell receptor-induced phosphorylation of the zeta chain is efficiently promoted by ZAP-70 but not Syk. *Blood* 104, Page 760-7.
- (25) Thome, M., Duplay, P., Guttinger, M., and Acuto, O. (1995) Syk and ZAP-70 mediate recruitment of p56lck/CD4 to the activated T cell receptor/CD3/zeta complex. *J Exp Med* 181, Page 1997-2006.
- (26) van Oers, N. S., Killeen, N., and Weiss, A. (1996) Lck regulates the tyrosine phosphorylation of the T cell receptor subunits and ZAP-70 in murine thymocytes. *J Exp Med* 183, Page 1053-62.
- (27) Mustelin, T. and K. Tasken, Positive and negative regulation of T-cell activation through kinases and phosphatases. *Biochem J*, 2003. 371(Pt 1): p. 15-27.

- (28) Weiss, A., Kadlecsek, T., Iwashima, M., Chan, A., and Van Oers, N. (1995) Molecular and genetic insights into T-cell antigen receptor signaling. *Ann N Y Acad Sci* 766, Page 149-56.
- (29) Ohteki, T., Parsons, M., Zakarian, A., Jones, R. G., Nguyen, L. T., Woodgett, J. R., and Ohashi, P. S. (2000) Negative regulation of T cell proliferation and interleukin 2 production by the serine threonine kinase GSK-3. *J Exp Med* 192, Page 99-104.
- (30) Davidson, D., Bakinowski, M., Thomas, M. L., Horejsi, V., and Veillette, A. (2003) Phosphorylation-dependent regulation of T-cell activation by PAG/Cbp, a lipid raft-associated transmembrane adaptor. *Mol Cell Biol* 23, Page 2017-28.
- (31) Marie-Cardine, A., Kirchgessner, H., Bruyns, E., Shevchenko, A., Mann, M., Autschbach, F., Ratnofsky, S., Meuer, S., and Schraven, B. (1999) SHP2-interacting transmembrane adaptor protein (SIT), a novel disulfide-linked dimer regulating human T cell activation. *J Exp Med* 189, Page 1181-94.
- (32) Maksumova, L., Le, H. T., Muratkhodjaev, F., Davidson, D., Veillette, A., and Pallen, C. J. (2005) Protein tyrosine phosphatase alpha regulates Fyn activity and Cbp/PAG phosphorylation in thymocyte lipid rafts. *J Immunol* 175, Page 7947-56.
- (33) Zheng, X. M., Resnick, R. J., and Shalloway, D. (2002) Mitotic activation of protein-tyrosine phosphatase alpha and regulation of its Src-mediated transforming activity by its sites of protein kinase C phosphorylation. *J Biol Chem* 277, Page 21922-9.

- (34) den Hertog, J., Tracy, S., and Hunter, T. (1994) Phosphorylation of receptor protein-tyrosine phosphatase alpha on Tyr789, a binding site for the SH3-SH2-SH3 adaptor protein GRB-2 in vivo. *EMBO J* 13, Page 3020-32.
- (35) Stetak, A., Csermely, P., Ullrich, A., and Keri, G. (2001) Physical and functional interactions between protein tyrosine phosphatase alpha, PI 3-kinase, and PKCdelta. *Biochem Biophys Res Commun* 288, Page 564-72.
- (36) Maksumova, L., Wang, Y., Wong, N. K., Le, H. T., Pallen, C. J., and Johnson, P. (2007) Differential function of PTPalpha and PTPalpha Y789F in T cells and regulation of PTPalpha phosphorylation at Tyr-789 by CD45. *J Biol Chem* 282, Page 20925-32.
- (37) 56. Wu, L., Yu, Z., and Shen, S. H. (2002) SKAP55 recruits to lipid rafts and positively mediates the MAPK pathway upon T cell receptor activation. *J Biol Chem* 277, Page 40420-7.
- (38) 57. Kliche, S., Breitling, D., Togni, M., Pusch, R., Heuer, K., Wang, X., Freund, C., Kasirer-Friede, A., Menasche, G., Koretzky, G. A., and Schraven, B. (2006) The ADAP/SKAP55 signaling module regulates T-cell receptor-mediated integrin activation through plasma membrane targeting of Rap1. *Mol Cell Biol* 26, Page 7130-44.
- (39) 58. Wang, H., and Rudd, C. E. (2008) SKAP-55, SKAP-55-related and ADAP adaptors modulate integrin-mediated immune-cell adhesion. *Trends Cell Biol* 18, Page 486-93.
- (40) 59. Maffucci, T., and Falasca, M. (2001) Specificity in pleckstrin homology (PH) domain membrane targeting: a role for a phosphoinositide-protein co-operative mechanism. *FEBS Lett* 506, Page 173-9.

- (41) 60. Storz, P., Doppler, H., Johannes, F. J., and Toker, A. (2003) Tyrosine phosphorylation of protein kinase D in the pleckstrin homology domain leads to activation. *J Biol Chem* 278, Page 17969-76.
- (42) 61. Bottino, C., Falco, M., Parolini, S., Marcenaro, E., Augugliaro, R., Sivori, S., Landi, E., Biassoni, R., Notarangelo, L. D., Moretta, L., and Moretta, A. (2001) NTB-A [correction of GNTB-A], a novel SH2D1A-associated surface molecule contributing to the inability of natural killer cells to kill Epstein-Barr virus-infected B cells in X-linked lymphoproliferative disease. *J Exp Med* 194, Page 235-46.
- (43) 62. Falco, M., Marcenaro, E., Romeo, E., Bellora, F., Marras, D., Vely, F., Ferracci, G., Moretta, L., Moretta, A., and Bottino, C. (2004) Homophilic interaction of NTBA, a member of the CD2 molecular family: induction of cytotoxicity and cytokine release in human NK cells. *Eur J Immunol* 34, Page 1663-72.
- (44) 63. Henel, G., Singh, K., Cui, D., Pryshchep, S., Lee, W. W., Weyand, C. M., and Goronzy, J. J. (2006) Uncoupling of T-cell effector functions by inhibitory killer immunoglobulin-like receptors. *Blood* 107, Page 4449-57.
- (45) 64. Tessmer, M. S., Fugere, C., Stevenaert, F., Naidenko, O. V., Chong, H. J., Leclercq, G., and Brossay, L. (2007) KLRG1 binds cadherins and preferentially associates with SHIP-1. *Int Immunol* 19, Page 391-400.
- (46) 4. Ficarro, S. B., McClelland, M. L., Stukenberg, P. T., Burke, D. J., Ross, M. M., Shabanowitz, J., Hunt, D. F., and White, F. M. (2002) Phosphoproteome analysis by mass

spectrometry and its application to *Saccharomyces cerevisiae*. *Nat Biotechnol* 20, Page 301-5.

(47) 9. Brill, L. M., Salomon, A. R., Ficarro, S. B., Mukherji, M., Stettler-Gill, M., and Peters, E. C. (2004) Robust phosphoproteomic profiling of tyrosine phosphorylation sites from human T cells using immobilized metal affinity chromatography and tandem mass spectrometry. *Anal Chem* 76, Page 2763-72.

(48) 10. Cao, L., Yu, K., Banh, C., Nguyen, V., Ritz, A., Raphael, B. J., Kawakami, Y., Kawakami, T., and Salomon, A. R. (2007) Quantitative time-resolved phosphoproteomic analysis of mast cell signaling. *J Immunol* 179, Page 5864-76.

(49) 11. Kruger, M., Kratchmarova, I., Blagoev, B., Tseng, Y. H., Kahn, C. R., and Mann, M. (2008) Dissection of the insulin signaling pathway via quantitative phosphoproteomics. *Proc Natl Acad Sci U S A* 105, Page 2451-6.

(50) 12. Schmelzle, K., Kane, S., Gridley, S., Lienhard, G. E., and White, F. M. (2006) Temporal dynamics of tyrosine phosphorylation in insulin signaling. *Diabetes* 55, Page 2171-9.

Chapter 5 Figure Legends

FIGURE 1. Canonical TCR signaling pathway. Established signaling cascades in activated T cells with quantitative Zap-70 null/Zap-70 reconstituted SILAC ratio data represented as heatmaps beside individual proteins. Heatmaps represent average of 5 replicate experiments. In the heatmap representation, green represents elevated phosphorylation in response to Zap-70 removal, while red represents a decrease in phosphorylation in response to Zap-70 removal. Black represents no change. Blanks in the heatmap indicate that a clearly defined SIC peak was not observed for that phosphopeptide in that time point. The utility of this visual representation is validated by the large number of red heatmap bars downstream of Zap-70 in the canonical pathway. Note that the * next to the phosphorylation site signifies that this site previously has been described in the literature.

FIGURE 2. Experimental procedure. Two cell populations of human Jurkat T cell clones (P116 and P116.c139) are incubated with normal or heavy isotope labeled arginine and lysine amino acids, physically differentiating the two proteomes by a shift in molecular weights. Each cell population is then pre-incubated with OKT3 and OKT4 antibodies for 10 minutes at 4 °C and then crosslinked with IgG at 37 °C for the times indicated. After cell lysis, samples are combined at an equal protein concentration ratio of 1:1. Samples are then reduced, alkylated, and trypsin-digested into peptides. Peptides are desalted by Sep-Pak cartridges and then enriched by phosphotyrosine peptide

immunoprecipitation and Fe³⁺ IMAC. Peptides are then subjected to reverse-phase LC-MS/MS analysis.

FIGURE 3. Quantitative phosphoproteomic analysis of known TCR signaling proteins in wild type cells. Listed above is a portion of the data collected, representing the known TCR signaling proteins that were observed in our study of human Jurkat P116.c139 (Zap-70 reconstituted) cells. Temporal quantitative changes in phosphorylation state are represented as heatmaps which represent average of 5 replicate experiments. In the heatmap representation, yellow represents levels of phosphorylation above the average, while blue represents levels of phosphorylation below the average. Black represents average abundance for a certain peptide across all time points. Blanks in the heatmap indicate that a clearly defined SIC peak was not observed for that phosphopeptide in that time point. Note that the * next to the phosphorylation site signifies that this site previously has been described in the literature.

FIGURE 4. Classification of ZAP-70 null/reconstituted SILAC ratios. The log₂ SILAC ratios of Zap-70 null to Zap-70 reconstituted cells were classified into 4 major categories: Peptides with substantially decreased phosphorylation; Peptides with decreased phosphorylation; Peptides with elevated phosphorylation; Peptides with no change in phosphorylation. SILAC ratios are calculated from the average of 5 replicate experiments.

FIGURE 5. Lck phosphorylation of the CD3 ζ ITAM motif requires Zap-70. A) TCR/CD3 Zap-70 null/Zap-70 reconstituted SILAC ratio profiles. Differences in phosphopeptide abundance over time were represented as SILAC ratios between P116 (Zap-70 null) and P116.c139 (Zap-70 reconstituted) cells on CD3 ζ , CD3 ϵ , and CD3 δ chains. SILAC ratios are calculated from the average of 5 replicate experiments. B) Model of Zap-70 dependent Lck phosphorylation of the CD3 ζ ITAM motif as well as CD3/CD4 antibody co-stimulation.

FIGURE 6. Dynamic effects of Zap-70 removal on novel phosphorylation sites discovered. Listed in this table is a subset of phosphorylation sites identified, representing the novel sites that displayed significant changes in response to Zap-70. Also included are the SILAC ratios (Zap-70 null/reconstituted) for the time points that showed significant changes amongst the 5 replicate experiments (p-value < 0.05) as well as the average SILAC ratio across the all time points. If missing data due to the sensitivity limit of the instrument prevented the reproducible observation of SILAC ratios in at least 3 replicate experiments, or the null hypothesis cannot be rejected, then those squares are left blank in this table.

FIGURE 7. Regulation of Fyn signaling. Model of Zap-70 dependent Fyn inhibition with quantitative Zap-70 null/Zap-70 reconstituted SILAC ratio data represented as

heatmaps beside individual proteins. Heatmaps are calculated from the average of 5 replicate experiments. Green represents elevated phosphorylation in response to Zap-70 removal, while red represents a decrease in phosphorylation in response to Zap-70 removal. Black represents no change. Blanks in the heatmap indicate that a clearly defined SIC peak was not observed for that phosphopeptide in that time point. Note that the * next to the phosphorylation site signifies that this site previously has been described in literature.

Supplemental Material 1. Disruption of Zap-70 from Jurkat cells and phosphorylation of Erk1/2. A) Zap-70 expression in Jurkat T cells. Protein lysates from P116 (Zap-70 null) and P116.c139 (Zap-70 reconstituted) were separated by SDS-Page and immunoblotted with Zap-70 specific antibodies. B) Erk1 and Erk2 phosphorylation in OKT3/OKT4 stimulated Jurkat T cells used in phosphoproteomic analysis. P116 (Zap-70 null) and P116.c139 (Zap-70 reconstituted) cells were stimulated with anti-CD3 (OKT3) and anti-CD4 (OKT4) antibodies. Protein lysates were then separated by SDS-Page and immunoblotted with phospho-p44/p42 MAPK (Erk1 and Erk2) specific antibodies.

Supplemental Material 2. Quantitative phosphoproteomic analysis of proteins not known to function in TCR signaling in wild type cells. Label free heatmap of a portion of the data collected, representing proteins that were observed in our study of human

Jurkat P116.c139 (Zap-70 reconstituted) cells not known to participate in the canonical T cell signaling pathway. Temporal quantitative changes in phosphorylation state are represented as heatmaps. Heatmaps are calculated from the average of 5 replicate experiments. Yellow represents levels of phosphorylation above the average, while blue represents levels of phosphorylation below the average. Black represents average abundance for a certain peptide across all time points. Blanks in the heatmap indicate that a clearly defined SIC peak was not observed for that phosphopeptide in that time point. Note that the * next to the phosphorylation site signifies that this site previously has been described in literature.

Supplemental Material 3. Zap-70 null to reconstituted SILAC ratio heatmap of proteins not known to function in TCR signaling in wild type cells. SILAC heatmap of a portion of the data collected, representing proteins that were observed in our study of human Jurkat P116.c139 (Zap-70 reconstituted) cells not known to participate in the canonical T cell signaling pathway. Zap-70 null/reconstituted SILAC ratios corresponding to the changes in phosphorylation state are represented as heatmaps. Heatmaps are calculated from the average of 5 replicate experiments. Green represents elevated phosphorylation in response to Zap-70 removal, while red represents a decrease in phosphorylation in response to Zap-70 removal. Blanks in the heatmap indicate that a clearly defined SIC peak was not observed for that phosphopeptide in that time point. Black represents no change. Note that the * next to the phosphorylation site signifies that this site previously has been described in the literature.

Chapter 6 Figures

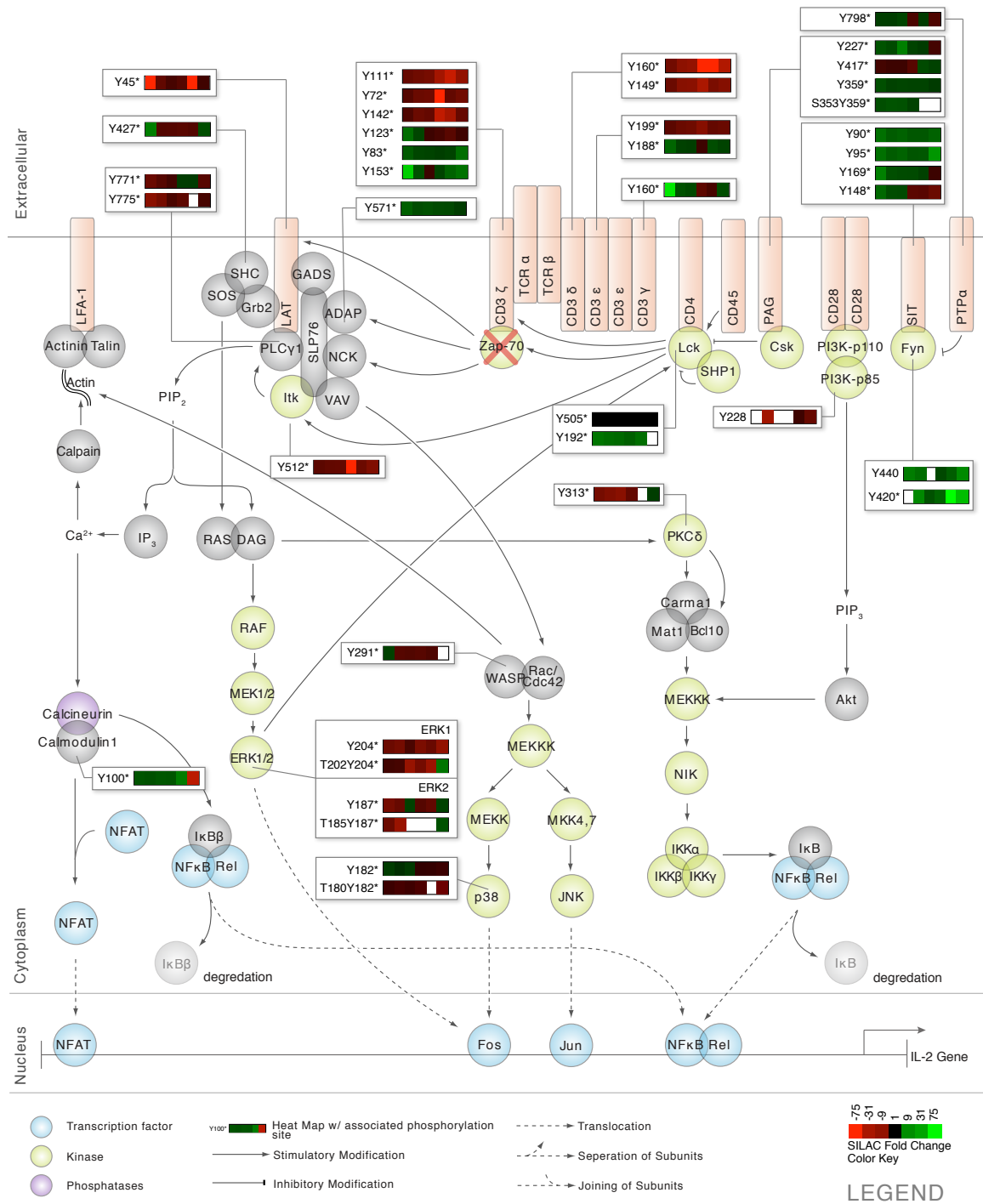


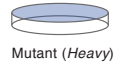
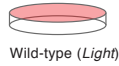
Figure 1

Label-Free Quantitation

Allows for comparison between multiple time points.

Experimental Procedure**SILAC Quantitation**

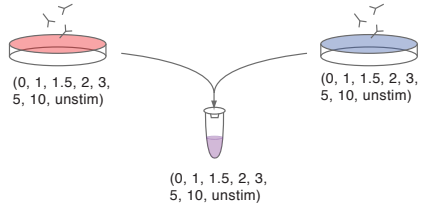
Allows for comparison between Wild-Type and Mutant cell lines

Cell Culture**Metabolic Labeling**

Label cells with *light* ($^{12}\text{C}, ^{14}\text{N}$) or *heavy* ($^{13}\text{C}, ^{15}\text{N}$) Arg and Lys.

Stimulation and Lysis

Cells are stimulated with CD3/4 + anti-IgG for 0, 1, 1.5, 2, 3, 5, 10 minutes. Unstimulated cells act as a control. Stimulation is halted by lysis.

**Combine**

Combine heavy and light lysates at a 1:1 ratio.

Trypsin Digestion

Equal amount of LIEDAEpYTAK peptide is added to each time point before immunoprecipitation.

Tyrosine-phosphorylated Peptide Enrichment

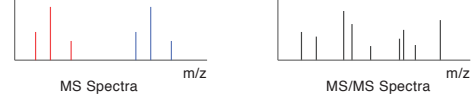
Phosphotyrosine immunoprecipitation and IMAC.



Peptide abundance between separate time points are normalized through the external standard peptide.

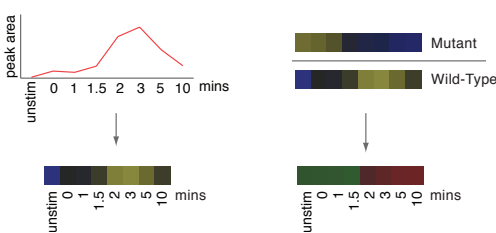
LC/MS/MS Data Acquisition

Spectra collected for peptides



Heavy and light peptides can be distinguished by mass shift created by incorporation of the isotope labeled amino acids.

Relative abundance heatmap generated based on peak area at each time point for each peptide. Blue (*yellow*) denotes lower (*higher*) than average peptide abundance.

Heatmap Generation

Ratio heatmaps generated based on the ratio of abundance between heavy and light peptide. Red (*green*) denotes decrease (*increase*) in peptide abundance in mutant cell lines at each time point.

Figure 2

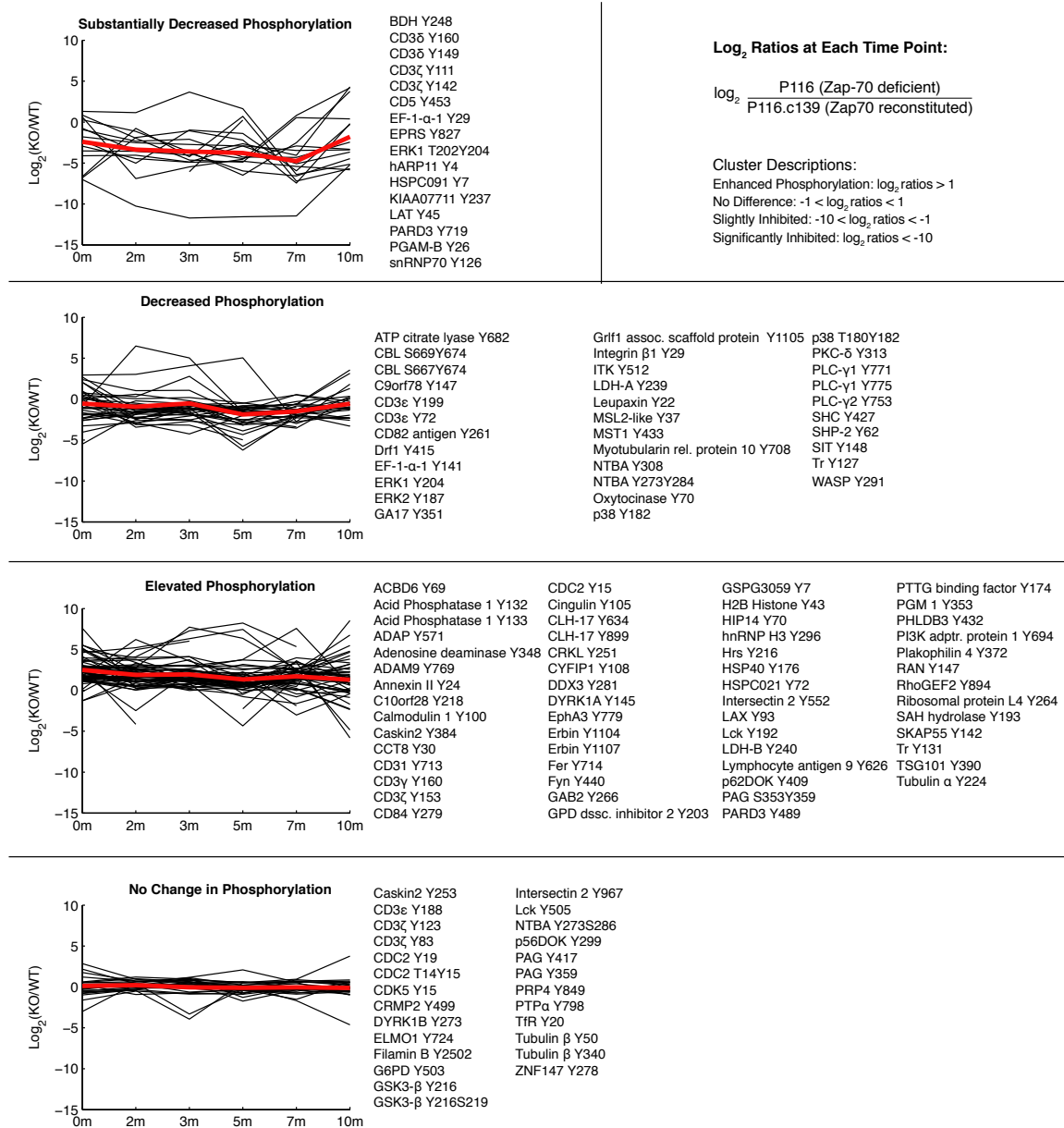


Figure 4

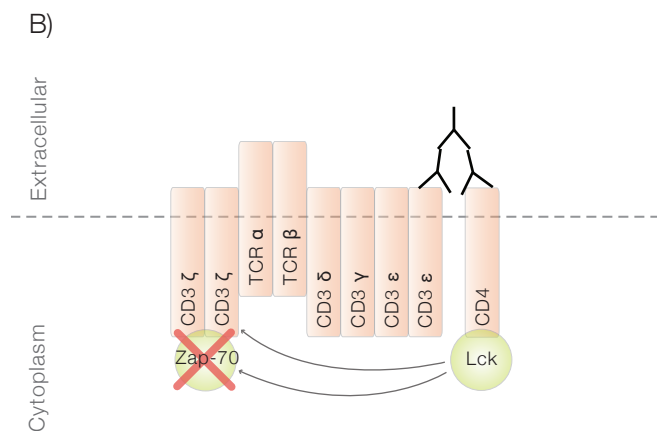
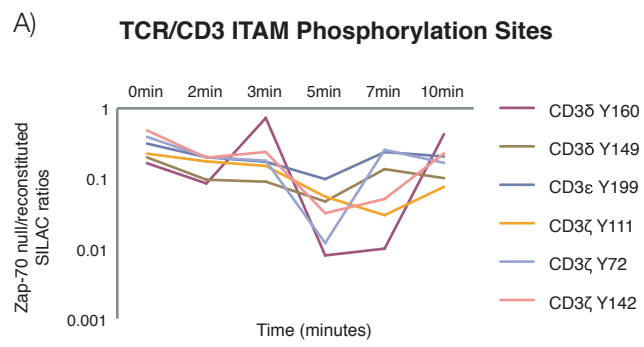


Figure 5

Name	Site	0 min	2 min	3 min	5 min	7 min	10 min	Avg. SILAC Ratio
ACBD6	Y69	16.37				15.73		16.05
Actin	Y93	1.94	1.45			2.70		2.03
ADAM9	Y769	37.11						37.11
Adenosine deaminase	Y348			2.53			2.29	2.41
ATP1A1	Y260			1.76				1.76
ATP1A3	Y548	0.74						0.74
ATP1A3	Y549	0.74						0.74
BDH	Y248		0.06		0.14			0.10
C10orf28	Y218	1.48						1.48
CCT8	Y30		4.79					4.79
CD7	Y222				0.54			0.54
CD84	Y279	4.82	2.19		3.19			3.40
CLH-17	Y634	5.93		7.05		8.56		7.18
CLH-17	Y899	6.36	8.14	8.35	6.34	10.05	6.69	7.65
CRMP2	Y499		2.02			0.62		1.32
DDX3	Y281	3.49						3.49
DDX49	Y223					2.82		2.82
Drf1	Y415	0.20	0.33				0.45	0.33
DYRK1A	Y145		8.09					8.09
EF-1- α -1	Y141	1.70						1.70
Elongation Protein 3	Y329	1.86		2.49	1.97			2.11
Enolase 2	Y44					3.97		3.97
Erbin	Y1107		10.31	1.92				6.12
G6PD	Y503					0.30		0.30
GA17	Y351				0.18			0.18
GDP dissociation inhibitor 2	Y203					3.54		3.54
Griff1 associated scaffold protein	Y237	12.65						12.65
GSPG3059	Y188	57.33						57.33
H2B Histone	Y43	3.43	6.34				0.02	3.26
H4 Histone	Y52	1.26	1.36					1.31
hARP11	Y4				0.01			0.01
Hrs	Y216		3.92		3.36			3.64
HSP40	Y176		3.34					3.34
HSP90B	Y484	1.81						1.81
HSPC021	Y72					145.62		145.62

Name	Site	0 min	2 min	3 min	5 min	7 min	10 min	Avg. SILAC Ratio
Intersectin 2	Y552					2.63		2.63
LAT	Y45		0.26					0.26
LDH-A	Y239	11.41	10.11					10.76
LDH-B	Y240	6.62	9.93		3.52	6.63		6.68
MSL2-like 1	Y37		0.36		0.37			0.36
MST1	Y433					0.25		0.25
Myotubularin related protein 10	Y708	0.14				0.64		0.39
Nephrin like 1	Y724	2.27						2.27
NTBA	Y308					0.54		0.54
Oxytocinase	Y70				0.19			0.19
PARD3	Y489					3.18		3.18
PARD3	Y719		0.03					0.03
PGAM-B	Y26	2.49	2.28					2.39
PGM 1	Y353	6.26				7.31		6.79
PHLDB3	Y432	6.42	3.94	3.38	1.73			3.87
PI3K adaptor protein 1	Y694		69.91	100.84			38.37	69.71
PI4K α	Y1096	7.05	8.45			7.18		7.56
Plakophilin 4	Y372		9.58					9.58
PTTG binding factor	Y174		36.77	77.03		16.02		43.28
RA-GEF-2	Y1447		2.60	3.02				2.81
RAN	Y147		9.28	9.30	9.93	10.98		9.87
RCC1 like	Y215		0.19		0.05			0.12
RhoGEF2	Y894	11.73	13.16	23.77	6.29	6.40	2.89	10.71
SAH hydrolase	Y193	15.70	15.62					15.66
SKAP55	Y142			5.78			3.28	4.53
STS1	Y19	3.84	1.38	1.50				2.24
Syntenin 1	Y56		20.46					20.46
Tec tyrosine kinase	Y519		1.39					1.39
Thioredoxin reductase 1	Y131	2.74	3.32	4.95		5.66	2.98	3.93
Tubulin alpha 1	Y224	197.19				2.76	10.81	70.25
Tubulin beta 1	Y50	0.81					0.64	0.72
Tubulin beta 1	Y340						0.69	0.69
TSG 101	Y390	4.08		3.13		2.55		3.25
ZNF404	Y312	0.56				2.42		1.49

Figure 6

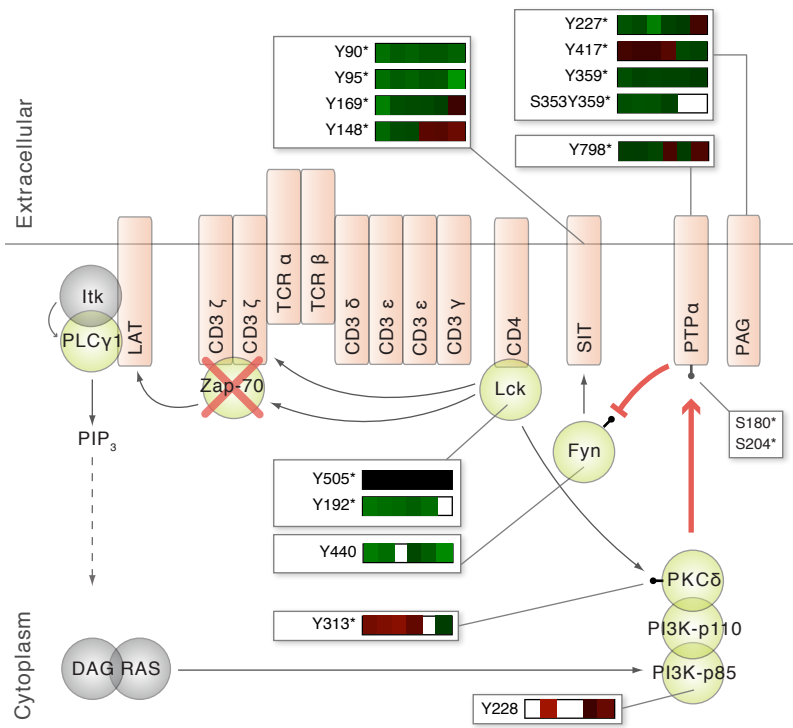
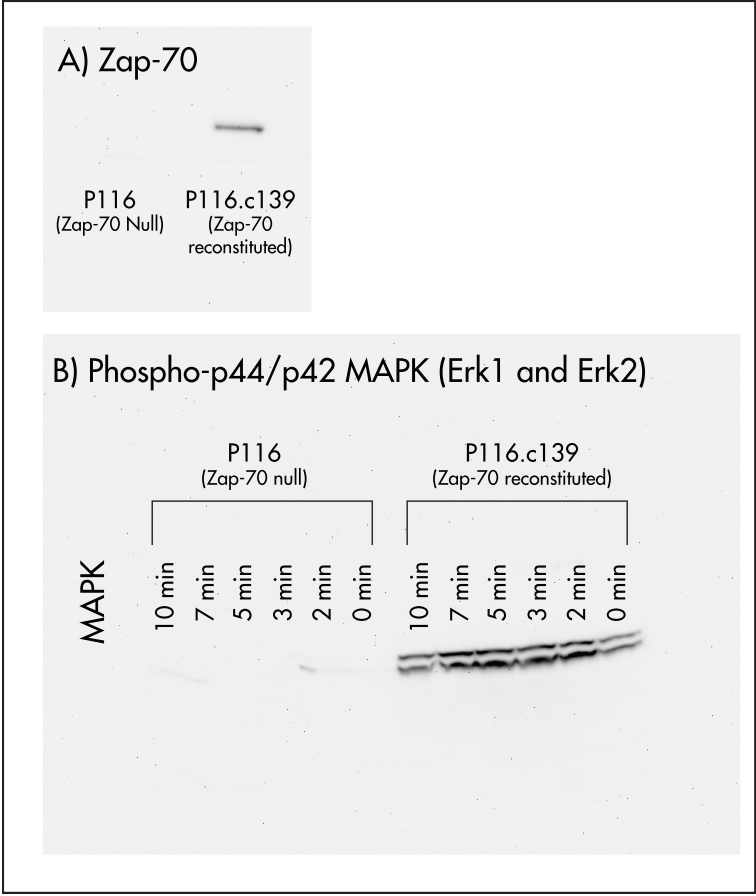


Figure 7



Supplemental Material 1



Protein Name	Phosphosites	mins					Protein Name	Phosphosites	mins					Protein Name	Phosphosites	mins				
		0	2	3	5	7			10	0	2	3	5			7	10	0	2	3
ACBD6	Y69						Enolase 2	Y44						Myotubularin rel protein 10	Y708					
Acid phosphatase 1	Y132*						EphA3	Y779*						Nephrin like 1	Y724					
Acid phosphatase 1	Y133*						EPRS	Y827						NTBA	Y308					
Actin	Y93						Erbin	Y1104*						NTBA	Y273Y284					
ADAM9	Y769						Erbin	Y1107						NTBA	Y273S286					
Adenosine deaminase	Y348						Fer	Y714*						Oxytocinase	Y70					
Annexin A11	Y279						Filamin B	Y2502						PARD3	Y489					
Annexin II	Y24*						G6PD	Y503						PARD3	Y719					
ATP citrate lyase	Y682						GA17	Y351						PGAM-B	Y26					
ATP1A1	Y260						GAB2	Y266*						PGM 1	Y353					
ATP1A3	Y548						GDP dissoc. inhibitor 2	Y203						PHLDB3	Y432					
ATP1A3	Y549						Golgin 84	Y54*						PI3K adaptor protein 1	Y694					
Bcl-2 modifying factor	Y1						GRF1	Y1105*						PI4Ka	Y1096					
BDH	Y248						Grif1 assoc. scaffold protein	Y237						Plakophilin 4	Y415*					
C10orf28	Y218						GSPG3059	Y188						Plakophilin 4	Y372					
C9orf78	Y147						H2B Histone	Y43						PLC-γ2	Y753*					
Caskin2	Y253						H4 Histone	Y52						PRP4	Y849*					
Caskin2	Y384*						hARP11	Y4						PTTG binding factor	Y174					
CCT8	Y30						HIP14	Y70						Pyruvate kinase 3	Y105					
CD31	Y713*						hnRNP H3	Y296						RAN	Y147					
CD7	Y222						hnRNP U like 1	Y510*						RCC1 like	Y215					
CD82 antigen	Y261						Hrs	Y216						RhoGEF2	Y894					
CDC2	Y15*						HSP40	Y176						Ribosomal protein L4	Y264					
CDC2	Y19						Hsp70	Y336						SAH Hydrolase	Y193					
CDC2	T14*Y15*						HSP90B	Y484						snRNP70	Y126					
Cingulin	Y105						HSPC021	Y72						STAM2	Y371*					
CLH-17	Y634						HSPC091	Y155						STS1	Y19					
CLH-17	Y899						Integrin beta 1	Y29						Syntenin 1	Y56					
CRKL	Y251*						Intersectin 2	Y967*						Tec tyrosine kinase	Y519					
CRMP2	Y499						Intersectin 2	Y552						Thioredoxin reductase 1	Y131					
CYFIP1	Y108						KIAA07711	Y237						Thioredoxin reductase 1	Y127					
DDX3	Y281						LAX	Y93						Transferrin receptor	Y20*					
DDX49	Y223						LDH-A	Y10						Tubulin alpha 1	Y272*					
Drf1	Y415						LDH-A	Y239						Tubulin alpha 1	Y224					
DYRK1A	Y145						LDH-B	Y240						Tubulin beta 1	Y50					
DYRK1B	Y273*						Leupaxin	Y22*						Tubulin beta 1	Y340					
EF-1-α-1	Y141						Lymphocyte antigen 9	Y626						TSG 101	Y390					
EF-1-α-1	Y29						MPZL1	Y263*						WD repeat protein 1	Y238					
ELMO1	Y724						MSL2-like 1	Y37						ZNF147	Y278					
Elongation Protein 3	Y329						MST1	Y433						ZNF404	Y312					

Supplemental Figure 2



Protein Name	Phosphosites	mins					Protein Name	Phosphosites	mins					Protein Name	Phosphosites	mins				
		0	2	3	5	7			10	0	2	3	5			7	10	0	2	3
ACBD6	Y69						Enolase 2	Y44						Myotubularin rel. protein 10	Y708					
Acid phosphatase 1	Y132*						EphA3	Y779*						Nephrin like 1	Y724					
Acid phosphatase 1	Y133*						EPRS	Y827						NTBA	Y308					
Actin	Y93						Erbin	Y1104*						NTBA	Y273Y284					
ADAM9	Y769						Erbin	Y1107						NTBA	Y273S286					
Adenosine deaminase	Y348						Fer	Y714*						Oxytocinase	Y70					
Annexin A11	Y279						Filamin B	Y2502						PARD3	Y489					
Annexin II	Y24*						G6PD	Y503						PARD3	Y719					
ATP citrate lyase	Y682						GA17	Y351						PGAM-B	Y26					
ATP1A1	Y260						GAB2	Y266*						PGM 1	Y353					
ATP1A3	Y548						GDP dissociation inhibitor 2	Y203						PHLDB3	Y432					
ATP1A3	Y549						Golgin 84	Y54*						PI3K adaptor protein 1	Y694					
Bcl-2 modifying factor	Y1						GRF1	Y1105*						PI4Ka	Y1096					
BDH	Y248						Griff1 associated scaffold protein	Y237						Plakophilin 4	Y415*					
C10orf28	Y218						GSPG3059	Y188						Plakophilin 4	Y372					
C9orf78	Y147						H2B Histone	Y43						PLC-gamma2	Y753*					
Caskin2	Y253						H4 Histone	Y52						PRP4	Y849*					
Caskin2	Y384*						hARP11	Y4						PTTG binding factor	Y174					
CCT8	Y30						HIP14	Y70						Pyruvate kinase 3	Y105					
CD31	Y713*						hnRNP H3	Y296						RAN	Y147					
CD7	Y222						hnRNP U like 1	Y510*						RCC1 like	Y215					
CD82 antigen	Y261						Hrs	Y216						RhoGEF2	Y894					
CDC2	Y15*						HSP40	Y176						Ribosomal protein L4	Y264					
CDC2	Y19						Hsp70	Y336						SAH Hydrolase	Y193					
CDC2	T14*Y15*						HSP90B	Y484						snRNP70	Y126					
Cingulin	Y105						HSPC021	Y72						STAM2	Y371*					
CLH-17	Y634						HSPC091	Y155						STS1	Y19					
CLH-17	Y899						Integrin beta 1	Y29						Syntenin 1	Y56					
CRKL	Y251*						Intersectin 2	Y967*						Tec tyrosine kinase	Y519					
CRMP2	Y499						Intersectin 2	Y552						Thioredoxin reductase 1	Y131					
CYFIP1	Y108						KIAA07711	Y237						Thioredoxin reductase 1	Y127					
DDX3	Y281						LAX	Y93						Transferrin receptor	Y20*					
DDX49	Y223						LDH-A	Y10						Tubulin alpha 1	Y272*					
Drf1	Y415						LDH-A	Y239						Tubulin alpha 1	Y224					
DYRK1A	Y145						LDH-B	Y240						Tubulin beta 1	Y50					
DYRK1B	Y273*						Leupaxin	Y22*						Tubulin beta 1	Y340					
EF-1-alpha-1	Y141						Lymphocyte antigen 9	Y626						TSG 101	Y390					
EF-1-alpha-1	Y29						MPZL1	Y263*						WD repeat protein 1	Y238					
ELMO1	Y724						MSL2-like 1	Y37						ZNF147	Y278					
Elongation Protein 3	Y329						MST1	Y433						ZNF404	Y312					

Supplemental Figure 3

Appendix I Interpretation of Quantitative Heatmaps

A label free data heatmap was generated for comparison of phosphopeptides in Zap-70 reconstituted Jurkat cells through a time course of receptor stimulation. The magnitude of change of the heatmap color was calculated from the log of the ratio of the fold change of each individual peptide peak area compared with the geometric mean for that peptide across all time points. Any changes (either an increase or decrease of peptide abundance above the average) with greater than 75 maximal fold change were displayed as the same color as the 75 maximal fold change. In the heatmap representation, the geometric mean of a given phosphopeptide across all time points was set to the color black. A blue color represented below average abundance, while yellow represented above average abundance for each unique phosphopeptide. Blanks in the heatmap indicated that a clearly defined SIC peak was not observed for that phosphopeptide in any of the replicate analyses for that time point. The heatmap colors were generated from the average of the LIEDAEPYTAK standard peptide normalized SICs in the 5 replicate experiments.

In the second type of heatmap, SILAC ratios corresponding to peptide abundance differences between Zap-70 null and reconstituted cell lines across the time course of receptor stimulation were represented. For the SILAC heatmaps, a black color represented a ratio of 1 between the two cell lines for a given peptide at that time point. A red color represented less abundance, and green represented higher abundance of the given peptide in the Zap-70 null cells compared to the Zap-70 reconstituted cells. The

heatmap color was thresholded at a maximal fold change of 75 fold increased or decreased in the Zap-70 null cells compared to reconstituted cells.